Self-Assembly of Chemically Linked Rod−Disc Mesogenic Liquid Crystals

Kwang-Un Jeong, Alexander J. Jing, Bart Monsdorf, Matthew J. Graham, Frank W. Harris, and Stephen Z. D. Cheng*

Maurice Morton Institute and Department of Polymer Science, The University of Akron, Akron, Ohio 44325-3909

Received: September 25, 2006; In Final Form: November 29, 2006

A series of new molecular discs (RD*n*, here *n* is the number of carbon atoms between the rod and disc mesogens) was synthesized via the chemical attachment of six cyanobiphenyl calamitic (rod) mesogens (R) linked to the triphenyl discotic (disc) mesogen (D) with a series of six alkyl chain linkages ($n = 6-12$). In this study, phase structures, transitions, and liquid crystalline (LC) behavior of the RD12 compound with 12 carbon atoms in each alkyl chain linkage between the rod and disc mesogens were investigated. Differential scanning calorimetry, polarized light microscopy, wide-angle X-ray diffraction (WAXD), and selected area electron diffraction (SAED) allowed us to identify three ordered phases below the isotropization temperature: nematic (N) LC and K_1 and K_2 crystalline phases. On the basis of the structural results obtained via 2D WAXD experiments on oriented samples and SAED experiments on single crystals, the K_1 crystalline unit cell was determined to be triclinic with the dimensions of $a = 1.36$ nm, $b = 1.45$ nm, $c = 2.11$ nm, $\alpha = 85°$, $\beta = 100°$, and $\gamma = 50°$. The K_2 phase was metastable with respect to the K_1 phase. It also possessed a triclinic unit cell with $a = 1.40$ nm, $b = 1.51$ nm, $c = 1.92$ nm, $\alpha = 87°$, $\beta = 117°$, and $\gamma = 62°$. Molecular packing models for the crystalline phases were proposed on the basis of the diffraction results. In the whole range of ordered structures, it was found that RD12 molecular discs are intercalated. Both triphenyl discotic mesogens and cyanobiphenyl calamitic mesogens are completely interdigitated.

Introduction

Not only for scientific interest but also for their practical applications, liquid crystalline (LC) materials have been studied for several decades. LC phases are defined as mesophases between three-dimensionally (3D) long-range ordered crystalline solids and 3D short-range ordered isotropic liquids.[1] The long-range order in LC phases is partly lost due to the mobility of the constituent building blocks. The combination of order and mobility in these soft materials leads to novel functional properties useful in electro-optical applications and in the field of life science.[2−9]

Both the mesogenic groups and the flexible tails can be designed to tune important LC properties.[10−12] Standard mesogens are either rod or disc shaped, while methylene or ethylene oxide segments are often used as flexible tails. To observe spontaneous electric polarization and hierarchical helical structures on the nanometer to micrometer length scales, for example, molecular chirality has been introduced to both the mesogenic groups and the flexible tails to break the symmetry of the LC building block.[13−18] Calamitic (rod) mesogens generally form nematic (N) and smectic LC phases, while discotic (disc) mesogens self-assemble into columnar N and columnar LC phases.[10−12] Unlike common rod LCs, which exhibit uniaxial positive birefringence, discotic LCs possess intrinsic uniaxial negative birefringence due to their disclike molecular shape. This enables these molecules to be useful in developing compensation films with a tilted optical axis and negative birefringence to improve the viewing angle of LC displays. They can also be utilized in field-effect transistors and photovoltaic devices due to their extraordinary one-dimensional (1D) electrical/photo conductivity.[19−23]

These basic rod and disc molecular structures can be further modified giving rise to controlled structural features in the mesophases. These modifications include using amphiphilic molecules,[24] block copolymers,[25] oligomers,[26] dendrimers,[27,28] metal-containing molecules,[29] achiral bent-core molecules,[30−32] and supramolecular systems.[33−37] The basic driving forces for controlling the formation of LC phases include not only molecular shape and space filling effects, but also the nanophase separation of incompatible constituents within and among molecules on the nanometer scale along with the minimization of interfaces between these nanophase separated structures.

Up to now, several combinations of rod and disc mesogens have been synthesized into both asymmetric and symmetric molecular structures.[38−42] For example, rodlike mesogens have been end-on and side-on attached to disclike mesogens. Another is disclike mesogens attached to rigid-rod backbone polymer chains. In this publication, we demonstrate the construction of newly designed molecular discs. This series of new molecular discs (RD*n*, here *n* is the number of carbon atoms between rod and disc mesogens) has been synthesized via the chemical linking of each of six cyanobiphenyl rod mesogens (R) to the triphenyl disc-like mesogenic group (D) by means of alkyl chains ($n = 6-12$). In this study, the RD12 compound with 12 carbon atoms in each of the alkyl chain linkages between the rod and the disc mesogens is used to represent the phase structures and transition behavior of this newly synthesized series.

RD12 was first characterized utilizing the combined techniques of differential scanning calorimetry (DSC), polarized light microscopy (PLM), wide-angle X-ray diffraction (WAXD), and

* To whom correspondence should be addressed. E-mail: scheng@uakron.edu.

10.1021/jp066274b CCC: $37.00
Published on Web 01/09/2007

SCHEME 1

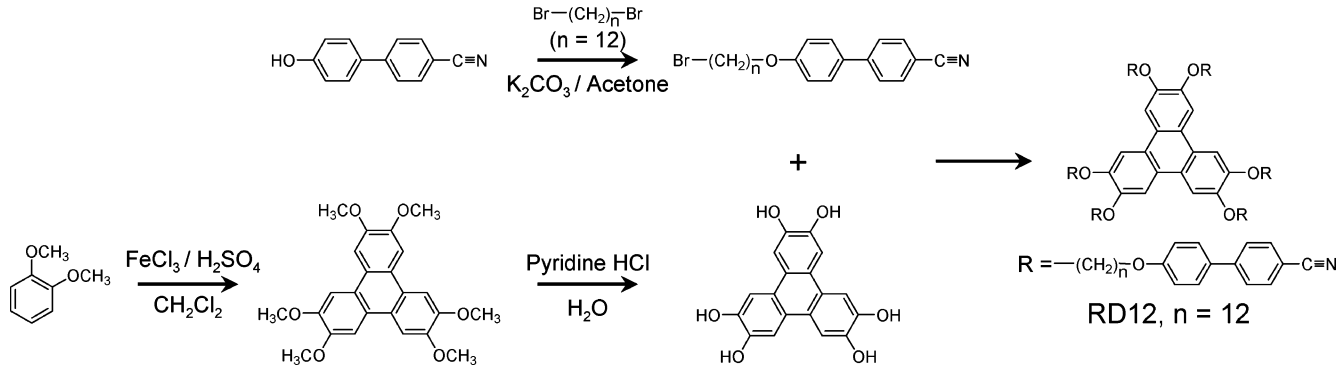

selected area electron diffraction (SAED) methods. On the basis of our experimental observations, we can conclude that there are three ordered phases in RD12 including one LC phase (N) and two crystalline phases (K_1 and K_2). Specifically designed experiments using DSC, 1D WAXD, and PLM allow us to determine that the K_2 phase formed when heating quenched RD12 is metastable with respect to the K_1 phase. A proposed RD 12 packing model has the discs intercalated in the ordered structure. Both the triphenyl discotic mesogens and the cyanobiphenyl calamitic mesogens are interdigitated.

Experimental Section

Materials and Sample Preparation. The RD*n* series of rod−disc LCs was synthesized via a four-step condensation reaction as shown in Scheme 1.[43] RD12 with 12 carbon atoms in each alkyl chain linkage between the rod and the disc mesogens was chosen for this study. The molecular weight of RD12 was 2490 g/mol. The calculated diameter of the triphenyl discotic core was 1.02 nm, and the length of each cyanobiphenyl rod was 1.07 nm. Assuming an all-*trans* conformation in the alkyl chains between the six rods and one disc, the diameter of RD12 molecular disc was 6.32 nm in vacuum based on calculations. The compound was purified by chromatography on silica gel using a chloroform/hexane (6/1) mixed solvent as an eluent, and then vacuum-dried. The purity and chemical structure of the compound were verified by thin-layer chromatography, MALDI-TOF mass spectrometry, elemental analysis, and nuclear magnetic resonance spectroscopy.

The purified compound was kept in vacuum before characterization. For DSC experiments, the sample weight was about 2.0 mg, and the pan weights were kept constant with a precision of ±0.001 mg. To observe the evolution of different phase structures, structurally isotropic RD12 films with a thickness of 0.5 mm were prepared in the melt for 1D WAXD powder experiments.

In order to obtain detailed structure information via 2D WAXD experiments, two different methods were used to orient the RD12 sample: mechanical drawing and application of a magnetic field. In the latter case, glass capillaries were used to hold the samples. The diameter of the glass capillary was 1.5 mm with a 0.01 mm wall thickness. The powder samples were carefully placed into the capillaries and then melted without air bubbles.

Density measurements were carried out at room temperature using a Guy−Lussac-type specific gravity bottle (10 mL) which was calibrated using the ASTM D 369 method. Mixed solutions of KI/water/ethanol were used to measure the density of crystallized samples. The experimentally observed density values were used to judge the number of molecules in the crystalline unit cells.

Thin film samples were prepared for transmission electron microscopy (TEM) experiments by solution-casting a dilute RD12/chloroform solution (0.01 g/L) on a carbon-coated mica surface. The sample was heated on a hot stage (Mettler FP-90) to above the isotropization temperature (T_i = 130 °C) in a dry nitrogen atmosphere to remove the solvent, and then, the samples were subsequently cooled to preset temperatures for crystallization. The film thickness of the sample was around 100 nm. After crystallization was completed, the films were removed from the mica surface and floated on a water surface. They were then recovered using copper grids. In order to obtain the homeotropic arrangement of RD12 discs for SAED experiments, a dilute RD12/chloroform solution (0.01 g/L) was floated on a water surface, and the sample was directly recovered using carbon-coated copper grids.

Equipment and Experiments. The thermal transitions were studied using a Perkin-Elmer PYRIS Diamond DSC with an Intracooler 2P apparatus. The temperatures and heat flows were calibrated using material standards (benzoic acid and indium) at cooling and heating rates ranging from 1 to 40 °C/min. The heating experiments always preceded the cooling experiments in order to eliminate previous thermal histories, and the cooling and heating rates were kept identical. The transition temperatures were determined by measuring the onset and peak temperatures from both the cooling and heating scans at different rates.

The 1D WAXD experiments were conducted in the reflection mode of a Rigaku 12 kW rotating-anode X-ray (Cu Kα radiation) generator coupled to a diffractometer. The diffraction peak positions and widths were calibrated with silicon crystals of known crystal size in the high 2θ-angle region (>15°) and silver behenate in the low 2θ-angle region. A hot stage was coupled to the diffractometer in order to study the structural evolutions with temperature changes during cooling and heating. The temperature of this hot stage was calibrated to be within ±1 °C. Samples were scanned across a 2θ-angle range from 1.5° to 35° at a scanning rate of 4°/min.

In order to obtain crystal unit cell dimensions and symmetry, 2D WAXD experiments on the oriented samples were conducted using an imaging system (Rigaku, R-AXIS-IV) with an 18 kW rotating anode X-ray generator. The 2D WAXD patterns were also calibrated via the same procedure as in the 1D WAXD experiments. A hot stage was also used to obtain diffraction patterns in the LC phase at elevated temperatures. A 30 min exposure time was required for a high-quality pattern. In both 1D and 2D WAXD experiments, background scatterings were subtracted from the sample scans.

TEM (FEI Tacnai 12) experiments were carried out to examine crystal morphology on the nanometer scale using an accelerating voltage of 120 kV. To achieve a higher contrast in the TEM micrograph, the samples were shadowed by Pt at a

tilting angle of 25°. SAED patterns of different zones were also obtained by tilting the single crystals in the samples. The camera length was set at 3.0 m. Calibration of the SAED spacing values smaller than 0.384 nm was carried out using evaporated thallous chloride, which has a largest first-order spacing diffraction of 0.384 nm. Spacing values larger than 0.384 nm were calibrated by doubling the *d*-spacing values of the first-order diffractions. The polyethylene (PE) surface lamellar decoration technique was applied to investigate the surface topology of the self-assembled structure of RD12 in the thin films.[44−47] The linear PE used had a number average molecular weight of 17.3 kg/mol with a polydispersity of 1.11. The PE was degraded, evaporated, and deposited onto the self-assembled surfaces in vacuum.

Morphological observations on the micrometer scale were conducted using PLM (Olympus BH-2) coupled with a Mettler heating stage (FP-90). The temperature of this hot stage was calibrated to be within ±0.5 °C.

The Cerius^2 (version 4.6) simulation software from Accelrys was used to calculate the energy minimized geometry of the RD12 molecular disc in the isolated gas phase utilizing the COMPASS force field.

Results and Discussion

Thermal Transitions and Their Corresponding Structural Evolutions. Figure 1a shows a set of DSC cooling diagrams at different scanning rates for RD12. At cooling rates of 40, 20, 10, and 5 °C/min, only one exothermic transition at 130 °C with a heat of transition of 13.4 kJ/mol (5.38 J/g) can be observed along with a glass transition temperature (T_g) at ∼38 °C. At slower cooling rates of 2.5 and 1 °C/min, another broad exothermic process becomes visible between 110 and 70 °C. The onset temperature and the heat of transition of the higher temperature transition remain constant at all of these cooling rates, indicating that this transition is an equilibrium (or very close to equilibrium) transition. In most cases, this represents an isotropic (I) melt to a low-ordered LC phase transition.[48−56] For the lower temperature transition, the transition temperatures (both the peak and onset) and heat of transition are cooling rate dependent. This type of transition behavior is usually observed for a crystallization process.[48−56]

The subsequent DSC heating diagrams, at the same rates as the prior DSC cooling experiments (Figure 1a), are shown in Figure 1b. At the highest rate of 40 °C/min, the only thermal transition visible is the endothermic transition at 130 °C with a heat of transition of 13.4 kJ/mol. This corresponds to the higher temperature transition observed during cooling, i.e., the LC ↔ I transition. At a heating rate of 20 °C/min, a broad exothermic process is observed between 100 and 115 °C, followed by an endothermic peak at 121 °C, which represents the melting of the phase formed by this exothermic process. Upon further decrease of the heating rate to 10, 5, 2.5, and 1 °C/min, a rate dependent exothermic process appeared between 60 and 110 °C. The endothermic peaks in these DSC heating diagrams were always at 121 °C. Because these heats of transition are relatively large between 67 and 95 kJ/mol, the transition should be a crystal melting process. After the exothermic process during heating at the rates of 2.5 and 5 °C/min, a very small endothermic peak appeared at ∼93 °C should reveal a fine structural change. The crystals then melt at 121 °C, and RD12 enters the LC phase before reaching the I melt.

Furthermore, the small heat of crystallization of the lower temperature transition (−14 kJ/mol) at the heating rate of 1 °C/min in Figure 1b is due to the fact that the majority of

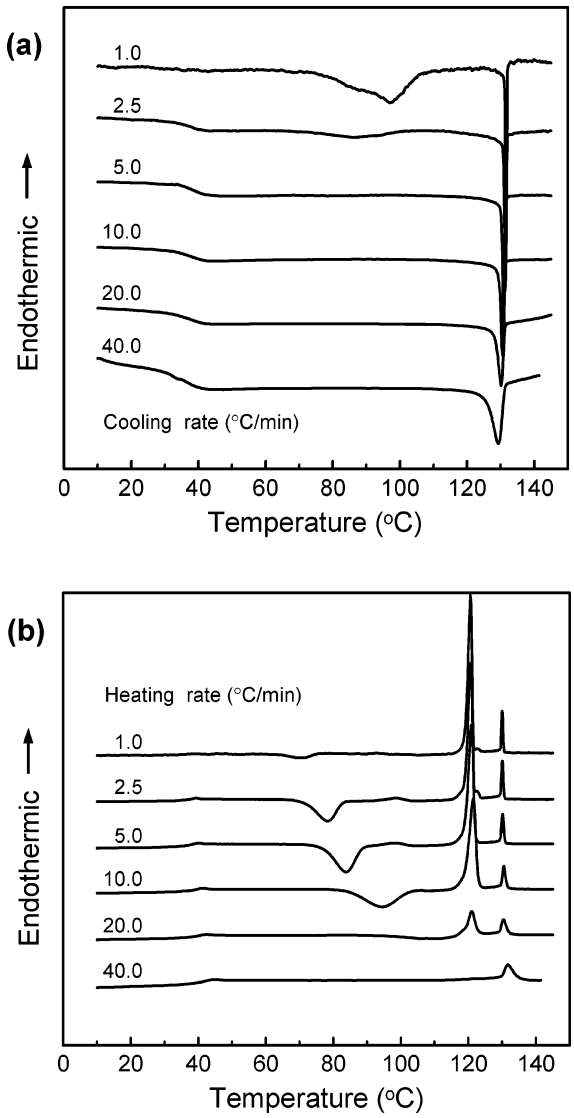

Figure 1. Two sets of DSC (a) cooling and (b) subsequent heating thermal diagrams for the RD12 compound at different rates between 1 and 40 °C/min.

RD12 has been crystallized in the previous cooling process at the identical rate of 1 °C/min (see Figure 1a). With increasing cooling rate (Figure 1a), the opportunity for RD12 crystallization decreases as evidenced by a decrease of the heat of transition in the lower temperature exothermic process in Figure 1a, and thus, the exothermic heat of transition in the subsequent heating in Figure 1b increases. Further increasing the cooling and heating rates results in hampering the crystallization as shown in the cases of 20 °C/min and, more evidently, at 40 °C/min (Figures 1a and 1b).

Although DSC experiments are sensitive to heat absorption and release events, this technique cannot provide direct information about structural changes. Therefore, 1D WAXD experiments at different temperatures are utilized to identify the corresponding structural evolutions.

Figure 2a shows a set of 1D WAXD patterns obtained by cooling RD12 from 137 °C (in the I melt) at a rate of 1 °C/min. In this figure, structures on two different length scales can be identified; one is on the nanometer scale in the low 2θ-angle region between 1.5° and 9°, and the other is on the subnanometer scale between 9° and 35°. At temperatures above 105 °C, only two amorphous halos are observed. Careful examination of these patterns indicates that, at 130 °C, a sudden

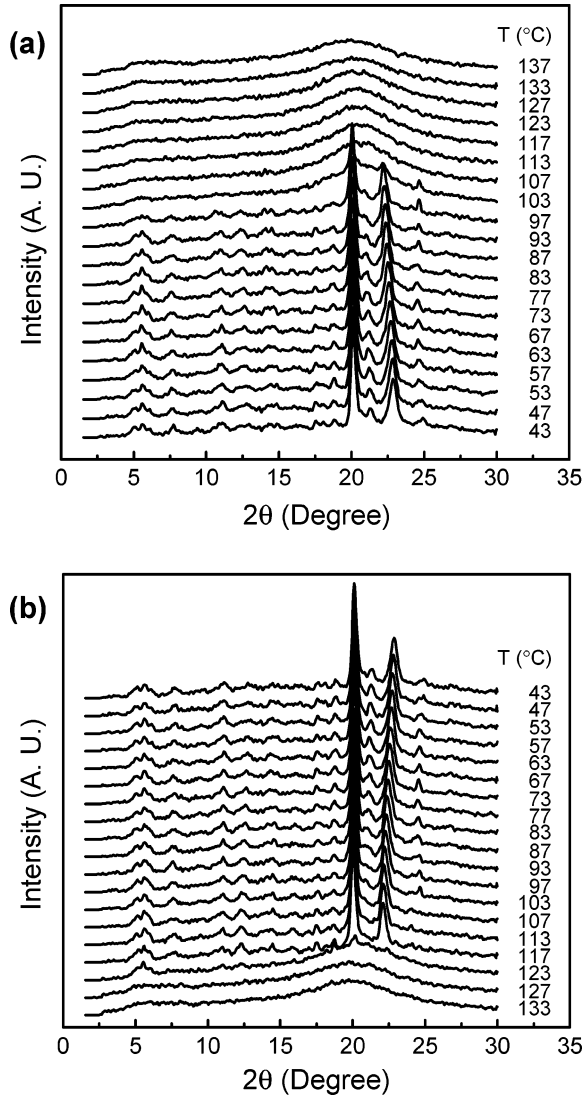

Figure 2. Two sets of 1D WAXD patterns of the RD12 at a (a) cooling and (b) subsequent heating rate of 1 °C/min at different temperatures.

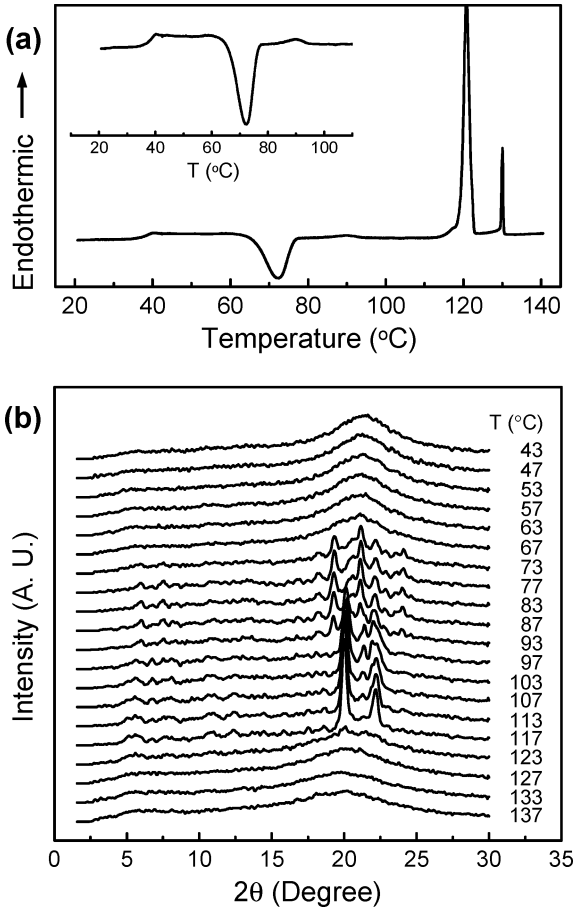

Figure 3. (a) DSC heating diagram of the RD12 at a heating rate of 1 °C/min after quenching the sample from 140 to 30 °C. The inset of Figure 3a is the enlarged DSC heating diagram of Figure 3a between 20 and 110 °C. (b) Set of 1D WAXD patterns of the RD12 at a heating rate of 1 °C/min at different temperatures after quenching the sample from 140 to 30 °C.

shift of the 2θ-angle of the halo from 20.0° (d-spacing = 0.444 nm) to 21.2° (d-spacing = 0.419 nm) occurs. This shift is typical of a transition from the I melt to a low-ordered N LC phase.[48−56] Therefore, the higher transition temperature in DSC (Figure 1a,b) is attributed to the I ↔ N LC phase transition. When the temperature is below 105 °C, multiple strong Bragg reflections appear. These reflections are associated with a crystalline structure, assigned as the K_1 phase. Further cooling does not result in any change of the 1D WAXD patterns. This observation agrees well with the DSC results at a cooling rate of 1 °C/min (Figure 1a). The subsequent heating experiment at 1 °C/min is shown in Figure 2b. The previously obtained diffraction pattern of the K_1 crystalline phase remains until 121 °C is reached. Above this temperature, the crystals melt, and the two amorphous halos appear, indicating an entrance into the N LC phase.

A remaining question is the following: Do the triphenyl discotic cores participate in forming this N phase? We can find the answer by further analyzing the heat of transition of the N LC ↔ I transition (13.4 kJ/mol in Figure 1a,b). The heat needed for the LC ↔ I melt transition of the cyanobiphenyl mesogen with 12 carbon atoms in a alkyl tail is ∼1.67 kJ/mol.[57] For six cyanobiphenyl mesogens in one RD12 compound, the overall contribution to the heat of transition is thus ∼10 kJ/mol. On the other hand, the heat of transition of the N LC ↔ I melt transition for pure triphenyl discotic LC compound is 3.4 kJ/mol.[58,59] Both parts of the heat of transition add up to ∼13.4 kJ/mol, which matches the heat of transition for the RD12 the LC ↔ I. Therefore, both cyanobiphenyl mesogens and triphenyl discotic cores in RD12 together construct this N LC phase.

In order to understand the small endothermic peak at ∼93 °C observed in the DSC heating diagram of Figure 1b and to evaluate the stability of the K_1 crystalline phase, a new DSC experiment was conducted. The sample was first quenched from the I melt at 140 °C to room temperature as rapidly as possible, and then, it was heated at 1 °C/min as shown in Figure 3a. Above the T_g at 38 °C, a large exothermic crystallization peak at 72 °C with a heat of transition of 74.2 kJ/mol appears followed by the small endothermic peat at 90 °C with a heat of transition of 4.4 kJ/mol. The higher temperature transition is at 121 °C, and the I ↔ N transition is at 130 °C, identical with the results of Figure 1b.

Figure 3b shows a set of 1D WAXD patterns to illustrate the corresponding structural evolutions of the quenched RD12 sample at different temperatures at a heating rate of 1 °C/min. Between 40 and 65 °C, the patterns are identical to that of the N LC phase at high temperatures, indicating that the N phase has been "frozen" by quenching the sample to below its T_g, and the K_1 structure does not have enough time to develop. By further increasing the temperature as shown in Figure 3b, RD12 starts to crystallize at ∼72 °C. A set of Bragg reflections develops, and they are different from the set of 1D WAXD

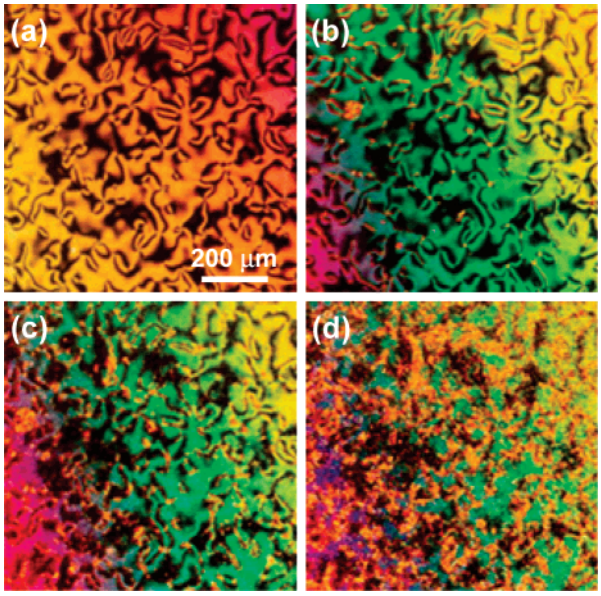

Figure 4. PLM textures of the RD12 at (a) 128, (b) 50, and (c) 30 °C upon cooling from isotropic state at 1 °C/min. (d) PLM texture of the RD12 at 65 °C upon subsequent heating at a rate of 1 °C/min from part c.

patterns obtained during cooling subsequently at 1 °C/min in Figure 2. Therefore, this new set of WAXD reflections must be associated with another crystalline phase, which is assigned as the K_2 crystalline phase. Moreover, the 1D WAXD pattern of the K_2 phase transfers into the K_1 phase at ~90 °C. This temperature corresponds to the DSC experimental observations in Figure 3a. Since the melting endothermic peak of the K_2 phase is very small in its heat of transition, it is predicted that the K_2 phase transferring to the K_1 phase is not a crystal melting/recrystallization mechanism, but rather, it is a solid−solid transition process with the small heat of transition. The K_1 crystalline phase again melts at 121 °C and enters the N LC phase as illustrated in the 1D WAXD patterns of Figure 3b.

Optical Texture Observations at Different Phases. Structural evolutions observed by the combination of DSC (Figures 1 and 3a) and 1D WAXD (Figures 2 and 3b) experiments can be supported by the texture changes observed in PLM. The optical textures of RD12 upon cooling at 1 °C/min from 140 to 30 °C have been recorded, and textures at three temperatures are shown in Figure 4a−c. The photograph taken at 128 °C (Figure 4a) shows the thread texture of the N LC phase.[60] With a further decrease of the temperature to 50 °C, small but highly birefringent aggregates appear which must be associated with the K_1 crystalline phase (Figure 4b). These aggregates grow continuously while cooling to 30 °C as shown in Figure 4c.

Subsequent heating processes were also recorded by PLM, as shown in Figure 4d at 65 °C after heating the sample of Figure 4c at 1 °C/min. The aggregates further develop in size, but the overall texture does not change. These PLM observations are consistent with the DSC (Figure 1) and 1D WAXD (Figure 2) results obtained at the 1 °C/min cooling and subsequent heating experiments. It should be noted that the birefringence of the photographs in Figure 4a is different from others. This change of color in birefringence may reflect a change in the thickness of the sample since the viscosity of the RD12 is low in the N LC phase. When the temperature is decreased, the sample solidifies, and the crystallization stops the flow of the sample. We also used 10 μm spacers to prevent the sample thickness from changing, and the birefringence color observed in PLM becomes consistent.

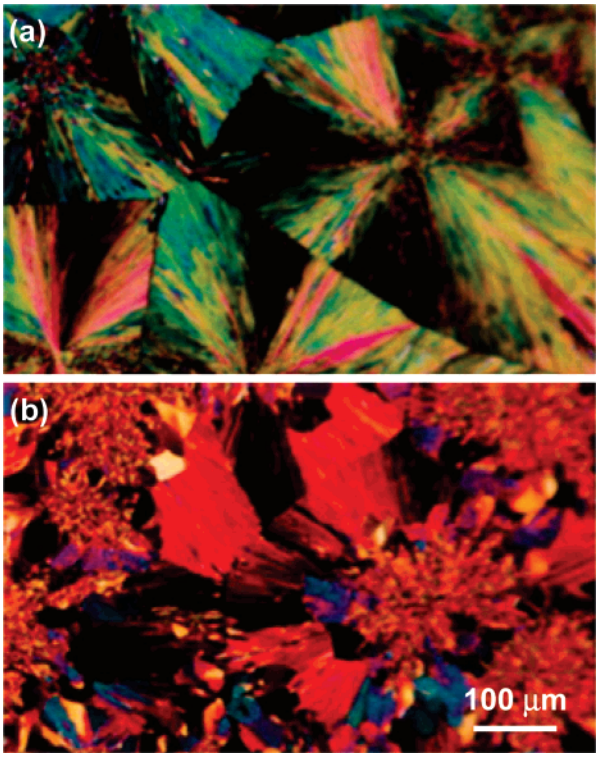

Figure 5. PLM textures of the RD12 (a) after quenching the sample from 128 °C to below the T_g, then heating it up to 75 °C, and (b) after annealing the sample from part a at 110 °C for 1 h.

The difference between the 1D WAXD patterns of the K_1 phase in Figure 2 and the K_2 phases in Figure 3b provides evidence that they represent two different crystalline structures. In order to distinguish the crystalline morphologies, we quenched RD12 from the N phase at 128 °C to below its T_g, and then heated it to 75 °C to generate the K_2 phase as shown in Figure 5a. The spherulitic texture is attributed to the K_2 crystalline phase. With subsequent annealing of the sample at 110 °C for 1 h, the K_1 crystalline phase formed aggregates of crystalline texture as shown in Figure 5b.

The phase transition behavior in RD12 is thus complex. The I melt first transfers to the N LC phase upon cooling at 130 °C, and this transition is thermodynamically reversible. The K_1 crystalline phase can be obtained by slow cooling the sample from the N LC phase. During heating, the K_1 crystalline phase melts at 121 °C and enters the N LC phase. On the other hand, the N LC phase can be "frozen" by fast quenching. The "frozen" N LC phase can further crystallize to form the K_2 crystalline phase upon heating. The K_2 crystalline phase then transfers to the K_1 crystalline phase at ~90 °C. Therefore, the K_2 crystalline phase formed by the quenching and subsequent heating is the metastable phase with respect to the K_1 crystalline phase.[61,62] The complete set of phase transition behaviors of RD12 is summarized in Figure 6.

Identifications of the Liquid Crystalline Phase Structure. Even though the 1D WAXD experiments at different temperatures combined with the DSC and PLM results can monitor the structural evolutions of RD12, 2D WAXD results from mechanically oriented samples and SAED from single crystals must be conducted to obtain detailed structural determination and symmetry. The oriented RD12 samples are prepared by drawing at 128 °C (in the N LC phase) and subsequently quenching to 30 °C. Its 2D WAXD pattern at 30 °C is shown in Figure 7a. The incident X-ray beam direction is normal to the fiber draw direction (the FD is along the meridian). In the

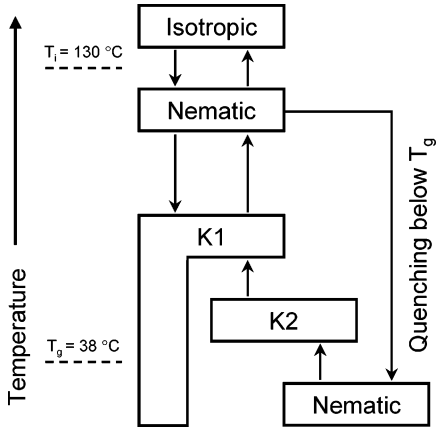

Figure 6. Phase transition diagram of the RD12 compound.

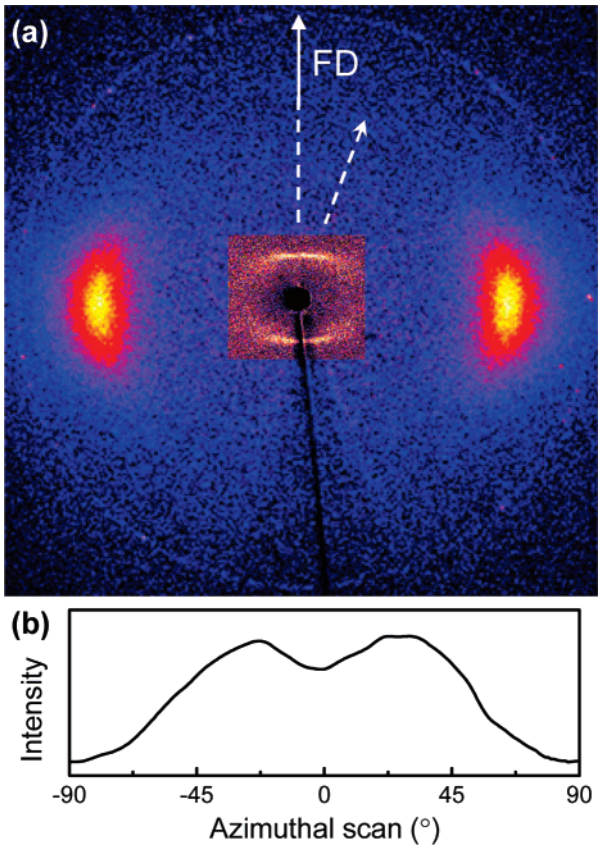

Figure 7. (a) Two-dimensional WAXD pattern of the N LC phase after being mechanically oriented at 128 °C and subsequent quenching the sample to 30 °C. (b) Azimuthal scan of the 2θ-angle between 3° and 8° of the 2D WAXD pattern (part a).

wide angle region, Figure 7a shows a pair of strong amorphous halos at $2\theta = 21.2°$ (d-spacing = 0.419 nm), where its maximum intensity is on the equator (perpendicular to the FD) with a correlation length of 2.1 nm as estimated by the Scherrer equation.[48−56] This indicates that the long axes of both the rod and the in-plane direction of the disc mesogens are along the drawn direction, and only short-range liquidlike order exists in the lateral packing of these mesogens. In the low angle region, one pair sharp arcs is observed at $2\theta = 5.0°$ (d-spacing = 1.77 nm). The maximum intensity of the reflections is in the quadrants at angles of $\sim\pm 20°$ of the meridian (Figure 7a), which is obvious in the azimuthal scan of the 2θ-angle between 3° and 8° (Figure 7b). This pair of the tilting angles with respect to the meridian (FD) depends on the quenching condition of

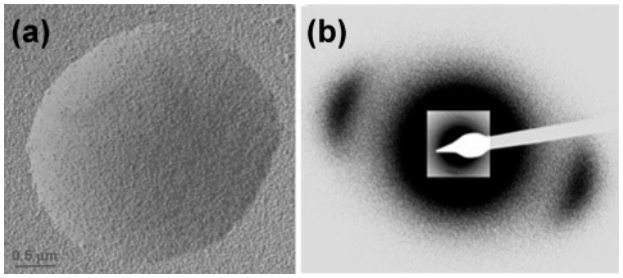

Figure 8. (a) TEM micrograph of RD12 after annealing at 128 °C and subsequently quenching the sample to 30 °C, while still in the N LC phase. (b) SAED pattern of the N LC phase.

the drawn fibers, and can vary in a range of ±5°. However, there are no second-order reflections for this pair of arcs.

This pair of the arcs tilting away from the meridian at $2\theta = 5.0°$ should be associated with the SmC-type cybotactic clusters formed while quenching the mechanically oriented sample. This type of phenomenon can be observed in some N LC phases.[63−65] Therefore, this phase should be assigned as an N LC phase rather than a stable smectic LC phase. Note that bent-core LCs also possess four off-meridian reflections in the low-angle region, and can be explained by the formation of a biaxial nematic LC phase.[66,67] If we assume that for each RD12 molecule the alkyl chains are in an all-*trans* conformation, the calculated diameter of the RD12 molecular disc is 6.32 nm, the calculated diameter of the triphenyl discotic core is 1.02 nm, the length of each cyanobiphenyl calamitic rod is 1.07 nm, and RD12 molecules are packed without intercalation. The model would generate a hexagonal packing with a d-spacing of 5.37 nm. This diffraction is not observed on the equator in 2D WAXD pattern of Figure 7a. Furthermore, the density of this packing is incorrect without overlapping of the entire disc with its neighbors. This indicates that a majority of the discotic mesogens and calamitic mesogens are intercalated. The reflections at $2\theta = 5.0°$ (d-spacing = 1.77 nm) in Figure 7a could be generated by the creation of the intercalated antiparallel cyanobiphenyl mesogens due to the strong dipole−dipole interaction. They also possess imperfect orientation.

This N LC phase structure can also be supported by SAED experiments. Figure 8a shows a bright-field image of a TEM micrograph of a single domain in the N LC phase, which was quenched from 128 to 30 °C after annealing in the N LC phase for 30 min. Its SAED is shown in Figure 8b. In addition to a pair of strong amorphous arcs at a d-spacing = 0.42 nm, a pair of relatively weak arcs at a d-spacing = 1.77 nm was observed, which matches the results of the 2D WAXD experiment (Figure 7a). These two pairs of arcs are not perpendicular to each other, but have an angle of 105°. This indicates that synclinically tilted SmC-type cybotactic clusters are created in the N LC phase of the oriented sample during the quench (Figure 7a). Combining both the 2D WAXD and SAED experimental results with the heat of transition data of the higher transition temperature, we can speculate that this N phase could be biaxial: one director is from the cyanobiphenyl calamitic rods and the other is from the triphenyl discotic core, which are orthogonal to each other.[38−42,68,69] The possible biaxiality of RD12 under an electric field is being studied.

In situ 2D WAXD experiments with a magnetic-field oriented RD12 sample at 128 °C was then carried out in order to support the explanation of the quenched samples. A constant magnetic field (**B**) of 1 T was utilized to orient the RD12 molecules at 128 °C in a glass capillary. A 2D WAXD pattern of the magnetic field oriented LC sample is shown in Figure 9. In the high angle

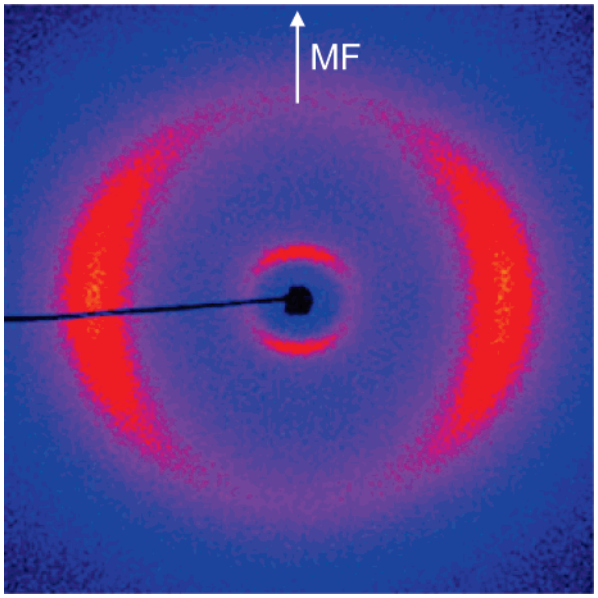

Figure 9. In situ 2D WAXD pattern of the N phase at 128 °C. The sample was oriented under a 1 T magnetic field.

region, a pair of strong amorphous halos at $2\theta = 21.2°$ (d-spacing = 0.42 nm) on the equator are identical to the quenched 2D WAXD fiber pattern (Figure 7a). In the low angle region, only a pair of strong amorphous halos appear on the meridian at $2\theta = 5.0°$ (d-spacing = 1.77 nm), not on the quadrants, which is close to the length of the intercalated antiparallel dimers of the cyanobiphenyl calamitic mesogen. This indicates that the synclinically tilted SmC-type cybotactic clusters are formed in the N LC phase of the mechanically oriented sample during the quenching process, which agrees well with the results from 2D WAXD (Figure 7a) and SAED (Figure 8b) of the quenched samples. It is particularly interesting that, in the N phase of RD12, the $\pi-\pi$ stacking between the triphenyl cores seems to be weak. The dominant driving forces for the self-assembly of the N phase in RD12 molecules are the microphase separation between the mesogens and alkyl chain linkages, and the interaction between the rod and disc-core.

Identifications of the Crystalline Phase Ordered Structures. For the determination of the stable K_1 crystalline structure, the oriented sample was prepared by heating up the quenched mechanically oriented sample to 110 °C at 1 °C/min followed by subsequent annealing at 110 °C for 5 h. A 2D WAXD pattern of this oriented RD12 sample is shown in Figure 10a. This pattern exhibits diffractions not only on the equator and meridian, but also in the quadrants, indicating formation of a 3D crystalline structure. In order to confirm this 2D WAXD pattern is from the K_1 crystalline phase, an azimuthal integration (360° β scan) was conducted to obtain the 1D WAXD pattern as shown in Figure 10b. This azimuthal integrated pattern is identical with the results of 1D WAXD powder pattern of the K_1 crystalline phase (Figures 2 and 3b). As indicated in Figure 10a, the c^* and b^* axes of the reciprocal lattice are off of both the meridian and the equator, and the a^* axis is along the equator (normal to the FD direction). Careful structural analysis of this 2D WAXD pattern in Figure 10a results in a triclinic unit cell of the K_1 crystalline phase with dimensions of $a = 1.36$ nm, $b = 1.45$ nm, $c = 2.11$ nm, $\alpha = 85°$, $\beta = 100°$, and $\gamma = 50°$ via refinement of the reciprocal lattice. The detailed determination procedure for a tricilinic unit cell can be found in ref 70. The experimentally observed 2θ values, d-spacings, and the calculated 2θ values based on this unit cell lattice are provided in Table 1. With one RD12 molecule in the triclinic unit cell, its calculated crystallographic density is 0.99 g/cm^3. The experimentally observed density is 0.97 g/cm^3, which fits well with the calculated data.

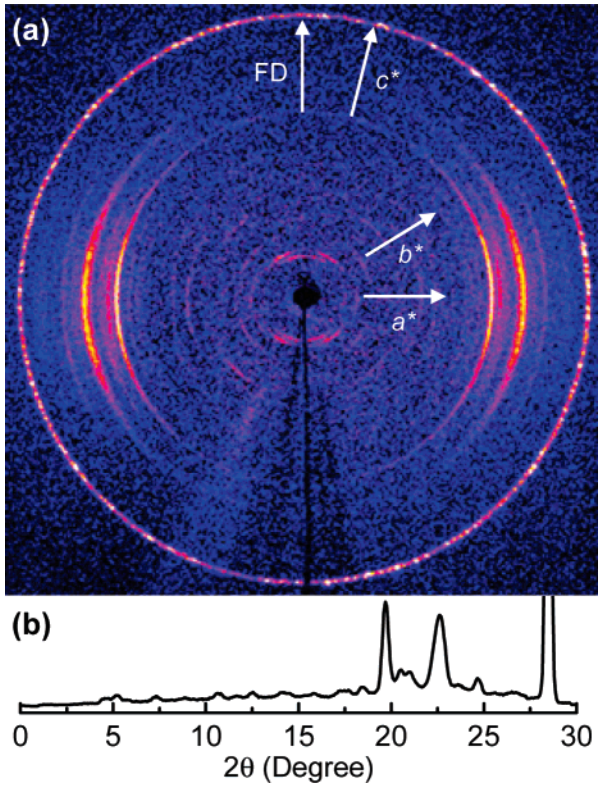

Figure 10. (a) Two-dimensional WAXD pattern of the K_1 phase. The sample was mechanically oriented at 128 °C and heated up to 110 °C at 1 °C/min, and then annealed at 110 °C for 5 h. (b) Azimuthal integrated WAXD from Figure 10a.

TABLE 1. Experimental and Calculated Crystallographic Parameters of the K_1 Crystalline Phase of RD12

	2θ (deg)		d-spacing (nm)	
hkl	expt[a]	calcd[b]	expt[a]	calcd[b]
001	4.41	4.41	2.00	2.01
110	6.98	6.98	1.27	1.27
010	8.26	8.25	1.07	1.07
100	8.90	8.90	0.99	0.99
002	8.81	8.82	0.99	1.00
$\bar{1}02$	10.5	10.5	0.84	0.84
003	13.2	13.3	0.68	0.67
$\bar{1}02$	14.3	14.3	0.62	0.62
$\bar{1}10$	15.8	15.7	0.56	0.56
020	16.5	16.5	0.54	0.54
$\bar{2}01$	17.1	17.0	0.52	0.52
$\bar{1}04$	17.4	17.3	0.51	0.51
004	17.6	17.7	0.50	0.50
200	18.0	17.9	0.49	0.50
$\bar{2}03$	18.8	18.8	0.47	0.47
131	19.5	19.6	0.45	0.45
321	21.3	21.2	0.42	0.42
104	22.1	22.1	0.41	0.40
$\bar{2}02$	22.3	22.2	0.40	0.40
$\bar{1}20$	23.5	23.6	0.38	0.38
$\bar{2}10$	24.5	24.3	0.36	0.37
$\bar{3}02$	25.5	25.7	0.36	0.35
$\bar{3}03$	26.4	26.2	0.34	0.34

[a] The accuracy of the experimental data is ±0.005 nm. [b] The calculated data listed are based on the K_1 triclinic unit cell with $a = 1.36$ nm, $b = 1.45$ nm, $c = 2.11$ nm, $\alpha = 85°$, $\beta = 100°$, and $\gamma = 50°$.

In order to confirm the structure determination based on this 2D WAXD pattern of the K_1 crystalline phase and to know the

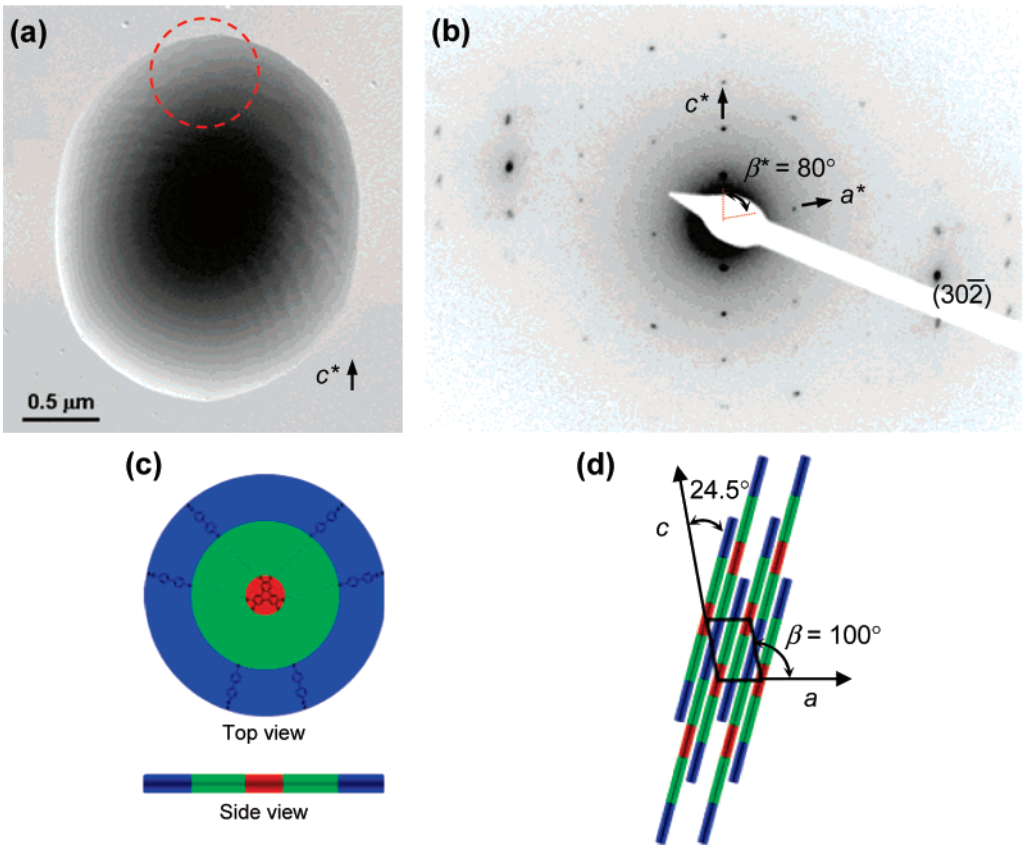

Figure 11. (a) TEM micrograph of RD12 after cooling from the N LC phase at 0.1 °C/min to 30 °C, and (b) its SAED pattern. SAED of part b was taken in the circle of part a. (c) Schematic illustrations of a RD12 molecule and (d) its molecular packing in the K_1 crystal.

molecular packing inside of the unit cell, TEM and SAED experiments from single crystals are required. Figure 11a shows a bright-field image of a single crystal in TEM which was grown by first annealing at 128 °C for 1 h and subsequently cooling down to 30 °C at a rate of 1 °C/min. On the basis of the previous results in DSC (Figure 1) and 1D WAXD (Figure 2), this single crystal is the K_1 crystalline phase. A SAED pattern of the K_1 phase is taken at the edge of the single crystal (the area in the circle of Figure 11a).

As indicated in Figure 11b, the β^* angle between the c^* axis and a^* axis is 80°. This is thus the [010] zone. Along the c^* axis of this SAED pattern, there are four pairs of diffraction spots with their d-spacing values multiples of each other, and they are the (001), (002), (003), and (004) diffractions with a d-spacing of 2.01 nm for the (001) diffraction. Along the a^* axis, a pair of diffractions at a d-spacing = 0.994 nm appears with weak second-order diffractions at d-spacing = 0.497 nm. They are assigned as the (100) and (200) diffractions, respectively. Therefore, the 2D unit cell dimension of the ac plane (a = 1.36 nm, c = 2.11 nm, and β = 100°) agrees well with the results from the 2D WAXD fiber pattern of the K_1 phase (Figure 10a). The overall diffractions on the SAED (Figure 11b) of the RD12 single crystal are asymmetric. The strongest diffractions in the short d-spacing values appear in the second and fourth quadrants (up-left and down-right quadrants). This reveals that RD12 discs (Figure 11c) are synclinically tilted clockwisely 24.5° from the c axis in the ac plane in real space. This is measured from the angle between the strong (30$\bar{2}$) pair of diffractions and a^* axis, as schematically illustrated in Figure 11d. Note that, in this model, the molecular disc plane is parallel to the (30$\bar{2}$) planes. The cyanobiphenyl mesogens overlap to form antiparallel arrangements due to the strong dipole−dipole interaction. This reveals that RD12 discs are intercalated, and

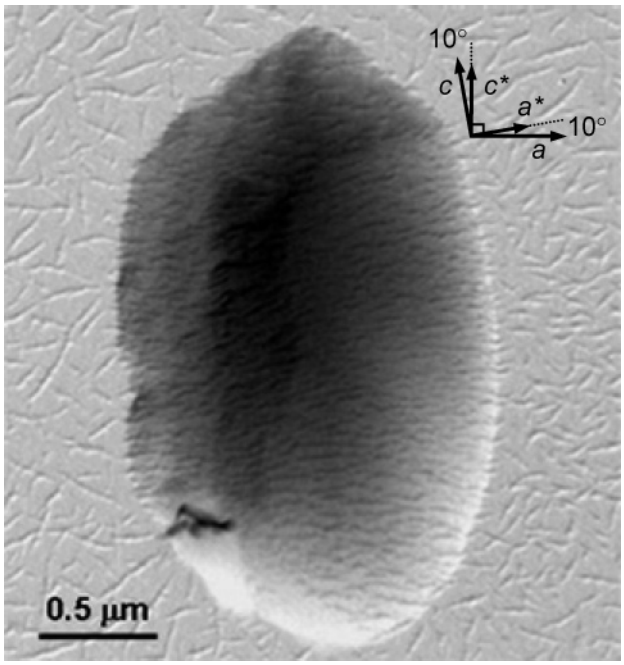

Figure 12. TEM micrograph after the PE surface lamellar decoration on the RD12 K_1 crystal surface.

the triphenyl discotic mesogens and the cyanobiphenyl calamitic mesogens are completely interdigitated in this K_1 crystalline phase. The intercalated RD12 disc packing model is schematically shown in Figure 11d in the ac plane in real space.

In order to support the intercalated RD12 disc packing model in the ac plane (along the [010] zone, see Figure 11d), the PE surface lamellar decoration experiment was conducted on the

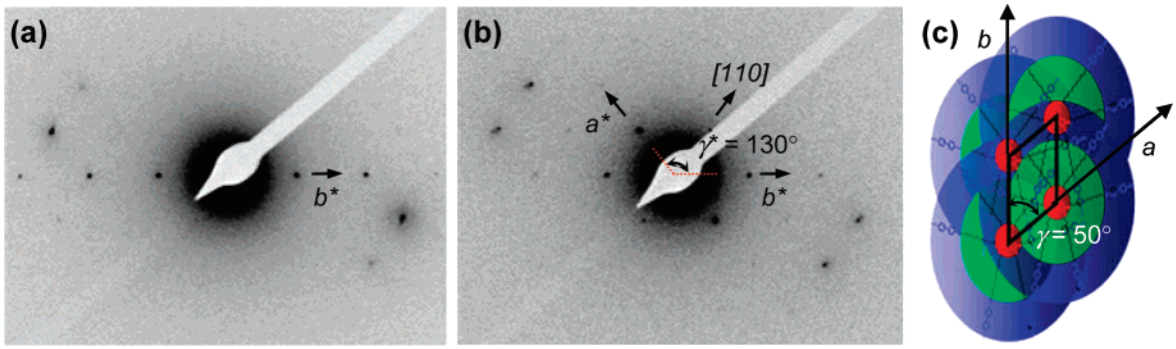

Figure 13. SAED patterns (a) without sample tilting and (b) with 5° counterclockwise tilting of the sample in part a around the [110] axis. (c) Schematic illustration of molecular packing along the [001] zone. The sample with a homeotropic arrangement was prepared by floating the dilute RD12/chloroform solution on the surface of water.

surface of the K_1 single crystals.[44−47] The result is shown in Figure 12. In this figure, the PE crystal rods are parallel to the a^* axis, which is perpendicular to the c axis as indicated in Figure 12. This indicates that the chain axes of the PE oligomers are deposited on the edge between the mesogens, and the PE chains are along the c axis. This surface topological information of the K_1 single crystal agrees with the proposed molecular packing model (Figure 11d).

In order to obtain the [001] zone SAED pattern of the K_1 crystal lattice, dilute RD12/chloroform solution (0.01 g/L) was floated on a water surface. After the chloroform solvent evaporated, the RD12 thin films on the water surface were directly recovered using carbon-coated copper grids on the water surface. Figure 13a shows an SAED pattern with the [301] zone in TEM without sample tilting. The [001] zone SAED pattern is obtained by tilting the [301] zone sample (Figure 13a) 5° counterclockwise around the [110] axis, as shown in Figure 13b. This [001] zone SAED pattern provides evidence of the intercalated RD12 disc molecular packing. The unit cell dimensions from this SAED pattern are $a = 1.36$ nm, $b = 1.45$ nm, and $\gamma = 50°$ (schematically illustrated in Figure 13c), which agree with those results deduced from the 2D WAXD fiber pattern (Figure 10a). The symmetry group of the K_1 phase was determined to be $P\bar{1}$ on the basis of the SAED results.

For the identification of the structure of the metastable K_2 crystalline phase, the quenched RD12 mechanically oriented sample was heated to 75 °C at 1 °C/min. The resulting 2D WAXD pattern of the oriented K_2 phase is shown in Figure 14a. The corresponding azimuthal integration (360° β scan) of this 2D WAXD (Figure 14b) was conducted to compare with the 1D WAXD pattern (Figure 3b), providing evidence that this 2D WAXD pattern represents the metastable K_2 crystalline phase. As indicated in Figure 14a, the c^* and b^* axes are also off of the meridian and the equator, and the a^* axis is along the equator. The molecular orientation in the K_2 phase is thus not much different from that of the K_1 phase. Careful structural analysis of the 2D WAXD pattern of the K_2 phase gives a triclinic unit cell with dimensions of $a = 1.40$ nm, $b = 1.51$ nm, $c = 1.92$ nm, $\alpha = 87°$, $\beta = 117°$, and $\gamma = 62°$ via the refinement of the reciprocal lattice.[70] The experimentally observed 2θ values and d-spacings and the calculated 2θ values as well as calculated d-spacings based on this unit cell lattice are provided in Table 2. With one RD12 disc in this triclinic unit cell, its calculated crystallographic density is 0.98 g/cm^3. The experimentally observed density is 0.96 g/cm^3, which fits with the calculated data.

This structural determination for the metastable K_2 crystalline phase is also obtained via a SAED experiment conducted on a RD12 single crystal. The K_2 single crystals were prepared by quenching the thin films from the N phase to room temperature followed by the subsequent heating up to 75 °C at 1 °C/min. The [010] zone SAED of the K_2 phase is obtained without sample tilting as shown in Figure 14c. The β^* angle is measured as 63° between the c^* axis and a^* axis, which agrees with the structural dimensions of the 2D WAXD pattern of the K_2 phase

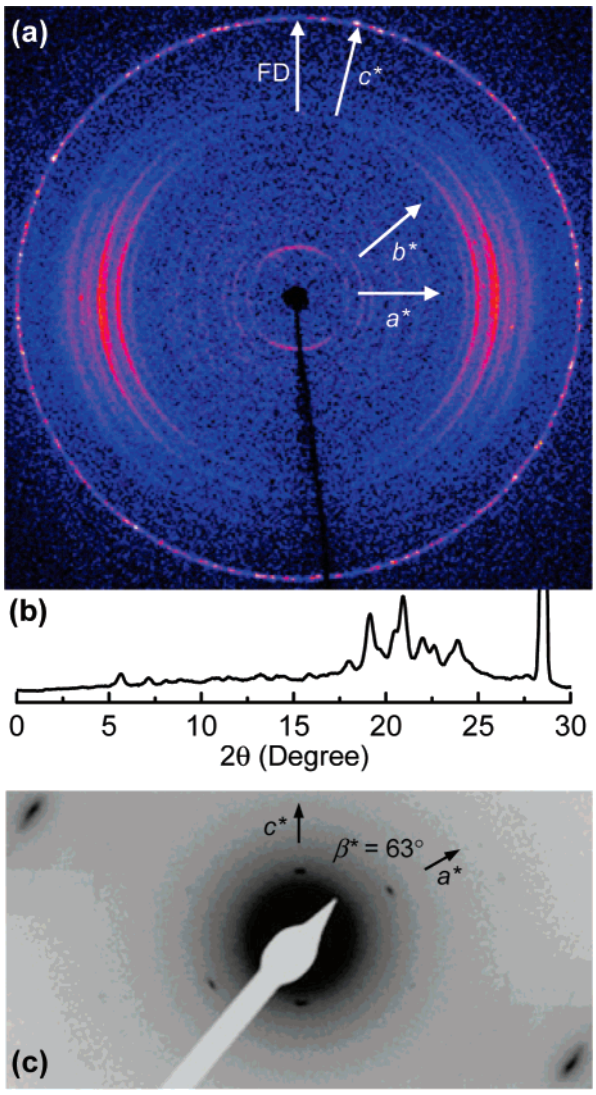

Figure 14. (a) Two-dimensional WAXD pattern of the K_2 phase. The sample was mechanically oriented at 128 °C followed by quenching, and then heated up to 75 °C at 1 °C/min. (b) Azimuthal integrated WAXD from part a. (c) SAED of K_2 single crystal obtained by heating the quenched sample up to 75 °C at 1 °C/min.

TABLE 2. Experimental and Calculated Crystallographic Parameters of the K_2 Crystalline Phase of RD12

	2θ (deg)		*d*-spacing (nm)	
hkl	expt[a]	calcd[b]	expt[a]	calcd[b]
001	5.50	5.49	1.60	1.61
010	7.03	7.04	1.27	1.26
100	8.52	8.52	1.04	1.04
002	11.1	11.0	0.81	0.81
200	17.0	17.1	0.53	0.52
131	18.0	18.0	0.49	0.49
231	19.9	19.9	0.45	0.45
$\bar{1}32$	19.7	19.7	0.44	0.45
$\bar{3}04$	23.2	23.1	0.39	0.39
$\bar{2}22$	24.0	24.2	0.37	0.37
$\bar{1}32$	24.3	24.4	0.37	0.36

[a] The accuracy of the experimental data is ±0.005 nm. [b] The calculated data listed are based on the K_2 triclinic unit cell with a = 1.40 nm, b = 1.51 nm, c = 1.92 nm, $\alpha = 87°$, $\beta = 117°$, and $\gamma = 62°$.

(Figure 14a). Along the c^* axis of this SAED pattern, there are a pair of diffraction spots with a d-spacing = 1.61 nm, which is identified as the (001) diffraction. A pair of diffractions at d-spacing = 1.04 nm also appears on the a^* axis. It is the (100) diffraction. Therefore, the 2D unit cell dimension of the [001] zone (a = 1.40 nm, c = 1.92 nm, and $\beta = 117°$) agrees with the results of the 2D WAXD fiber pattern of the K_2 phase (Figure 14a). The higher ordered diffractions are weak.

Conclusion

In summary, a new series of molecular discs was synthesized via the chemical attachment of the six cyanobiphenyl rod mesogen (R) to the periphery of a triphenyl disclike mesogen group (D) with six alkyl chain linkages having various carbons in each linkage. For RD12, three ordered phases below the isotropization temperature were identified utilizing results of the combined techniques of DSC, 1D WAXD, and PLM. They are the N LC phase as well as the K_1 and the K_2 crystalline phases. The K_1 phase is formed by slowly cooling the sample from the N phase, e.g., at 1 °C/ min. The K_2 phase is created by quenching from the N phase to room temperature and, then, heating it to a higher temperature (∼75 °C). The K_2 phase is metastable with respect to the stable K_1 phase. On the basis of the 2D WAXD experiments on oriented samples and SAED experiments on single crystals, the K_1 crystalline structure was determined to be triclinic with dimensions of a = 1.36 nm, b = 1.45 nm, c = 2.11 nm, $\alpha = 85°$, $\beta = 100°$, and $\gamma = 50°$, while the K_2 phase also possesses a triclinic unit cell with a = 1.40 nm, b = 1.51 nm, c = 1.92 nm, $\alpha = 87°$, $\beta = 117°$, and $\gamma = 62°$. Molecular packing models in the ordered phases are also proposed on the basis of the diffraction experiment results. In the whole range of ordered structures, RD12 molecular discs are intercalated, and both the triphenyl discotic mesogens and the cyanobiphenyl mesogens are completely mixed and interdigitated.

Acknowledgment. This work was supported by NSF DMR-0516602 and the Collaborative Center for Polymer Photonics between the Air Force Research Laboratory Materials and Manufacturing Directorate and The University of Akron. We also acknowledge Perkin-Elmer Co. in providing a Diamond DSC instrument in our laboratory.

References and Notes

(1) Goodby, J. W.; Gray, G. W. *Handbook of Liquid Crystals*; Demus, D., Goodby, J., Gray, G. W., Spiess, H.-W., Vill, V., Eds.; Wiley-VCH: Weinheim, 1998; Vol. 1, pp 17−23.
(2) Sage, I. C. *Handbook of Liquid Crystals*; Demus, D., Goodby, J., Gray, G. W., Spiess, H.-W., Vill, V., Eds.; Wiley-VCH: Weinheim, 1998; Vol. 1, pp 731−762.
(3) Crossland, W.; Wilkinson, T. D. *Handbook of Liquid Crystals*; Demus, D., Goodby, J., Gray, G. W., Spiess, H.-W., Vill, V., Eds.; Wiley-VCH: Weinheim, 1998; Vol. 1, pp 763−822.
(4) Hoffmann, S. *Handbook of Liquid Crystals*; Demus, D., Goodby, J., Gray, G. W., Spiess, H.-W., Vill, V., Eds.; Wiley-VCH: Weinheim, 1998; Vol. 3, pp 393−452.
(5) Ichimura, K. *Chem. Rev.* **2000**, *100*, 1847.
(6) Wang, L. Y.; Chen, X.; Zhan, J.; Chai, Y. C.; Yang, C. J.; Xu, L. M.; Zhuang, W. C.; Jing, B. *J. Phys. Chem. B* **2005**, *109*, 3189.
(7) Araos, M. U.; Warr, G. G. *J. Phys. Chem. B* **2005**, *109*, 14275.
(8) Hayer, A.; de Halleux, V.; Kohler, A.; El-Garoughy, A.; Meijer, E. W.; Barbera, J.; Tant, J.; Levin, J.; Lehmann, M.; Gierschner, J.; Cornil, J.; Geerts, Y. H. *J. Phys. Chem. B* **2006**, *110*, 7653.
(9) Lee, L. M.; Kwon, H. J.; Nuzzo, R. G.; Schweizer, K. S. *J. Phys. Chem. B* **2006**, *110*, 15782.
(10) Demus, D. *Handbook of Liquid Crystals*; Demus, D., Goodby, J., Gray, G. W., Spiess, H.-W., Vill, V., Eds.; Wiley-VCH: Weinheim, 1998; Vol. 1, pp 133−187.
(11) Tschierske, C. *J. Mater. Chem.* **1998**, *8*, 1485.
(12) Saez, I. M.; Goodby, J. W. *J. Mater. Chem.* **2005**, *15*, 26.
(13) Goodby, J. W. *Science* **1986**, *231*, 350.
(14) Goodby, J. W. *Handbook of Liquid Crystals*; Demus, D., Goodby, J., Gray, G. W., Spiess, H.-W., Vill, V., Eds.; Wiley-VCH: Weinheim, 1998; Vol. 1, pp 115−132.
(15) Li, C. Y.; Cheng, S. Z. D.; Ge, J. J.; Bai, F.; Zhang, J. Z.; Mann, I. K.; Harris, F. W.; Chien, L.-C.; Yan, D.; He, T.; Lotz, B. *Phys. Rev. Lett.* **1999**, *83*, 4558.
(16) Li, C. Y.; Cheng, S. Z. D.; Ge, J. J.; Bai, F.; Zhang, J. Z.; Mann, I. K.; Chien, L. C.; Harris, F. W.; Lotz, B. *J. Am. Chem. Soc.* **2000**, *122*, 72.
(17) Li, C. Y.; Cheng, S. Z. D.; Weng, X.; Ge, J. J.; Bai, F.; Zhang, J. Z.; Calhoun, B. H.; Harris, F. W.; Chien, L. C.; Lotz, B. *J. Am. Chem. Soc.* **2001**, *123*, 2462.
(18) Lotz, B.; Cheng, S. Z. D. *Polymer* **2005**, *46*, 577.
(19) Vaughan, G. B. M.; Heiney, P. A.; McCauley, J. P., Jr.; Smith, A. B., III. *Phys. Rev. B* **1992**, *46*, 2787.
(20) Adam, D.; Closs, F.; Frey, T.; Funhoff, D.; Haarer, D.; Ringsdorf, H.; Schuhmacher, P.; Siemensmeyer, K. *Phys. Rev. Lett.* **1993**, *70*, 457.
(21) Mori, H.; Itoh, Y.; Nishiura, Y.; Nakamura, T.; Shinagawa, Y. *Jpn. J. Appl. Phys.* **1997**, *36*, 143.
(22) Qi, M. H.; Liu, G. F. *J. Phys. Chem. B* **2003**, *107*, 7640.
(23) Ge, J. J.; Hong, S. C.; Tang, B. Y.; Li, C. Y.; Zhang, D.; Bai, T.; Mansdorf, B.; Harris, F. W.; Yang, D.; Shen, Y. R.; Cheng, S. Z. D. *Adv. Funct. Mater.* **2003**, *13*, 718.
(24) Carlsson, N.; Sanandaji, N.; Voinova, M.; Akerman, B. *Langmuir* **2006**, *22*, 4408.
(25) Tenneti, K. K.; Chen, X.; Li, C. Y.; Tu, Y.; Wan, X.; Zhou, Q.-F.; Sics, I.; Hsiao, B. S. *J. Am. Chem. Soc.* **2005**, *127*, 15481.
(26) Cui, L.; Miao, J.; Zhu, L.; Sics, I.; Hsiao, B. S. *Macromolecules* **2005**, *38*, 3386.
(27) Bobrovsky, A. Y.; Pakhomov, A. A.; Zhu, X. M.; Boiko, N. I.; Shibaev, V. P.; Stumpe, J. *J. Phys. Chem. B* **2002**, *106*, 540.
(28) Cho, B.-K.; Jain, A.; Mahajan, S.; Ow, H.; Gruner, S. M.; Wiesner, U. *J. Am. Chem. Soc.* **2004**, *126*, 4070.
(29) Cardinaels, T.; Driesen, K.; Parac-Vogt, T. N.; Heinrich, B.; Bourgogne, C.; Guillon, D.; Donnio, B.; Binnemans, K. *Chem. Mater.* **2005**, *17*, 6589.
(30) Niori, T.; Sekine, T.; Watanabe, J.; Furukawa, T.; Takezoe, H. *J. Mater. Chem.* **1996**, *6*, 1231.
(31) Link, D. R.; Natale, G.; Shao, R.; Mclennan, J. E.; Clark, N. A.; Korblova, E.; Walba, D. M. *Science* **1997**, *278*, 1924.
(32) Shen, D.; Pegenau, A.; Diele, S.; Wirth, I.; Tschierske, C. *J. Am. Chem. Soc.* **2000**, *122*, 1593.
(33) Dingemans, T. J.; Murthy, N. S.; Samulski, E. T. *J. Phys. Chem. B* **2001**, *105*, 8845.
(34) Jin, S.; Ma, Y.; Zimmerman, S. C.; Cheng, S. Z. D. *Chem. Mater.* **2004**, *16*, 2975.
(35) Jeong, K.-U.; Jin, S.; Ge, J. J.; Knapp, B. S.; Graham, M. J.; Ruan, J.; Guo, M.; Xiong, H.; Harris, F. W.; Cheng, S. Z. D. *Chem. Mater.* **2005**, *17*, 2852.
(36) Jeong, K.-U.; Knapp, B. S.; Ge, J. J.; Jin, S.; Graham, M. J.; Harris, F. W.; Cheng, S. Z. D. *Chem. Mater.* **2006**, *18*, 680.
(37) Shen, H.; Jeong, K.-U.; Xiong, H.; Graham, M. J.; Leng, S.; Zheng, J. X.; Huang, H.; Guo, M.; Harris, F. W.; Cheng, S. Z. D. *Soft Matter* **2006**, *2*, 232.
(38) Hunt, J. J.; Date, R. W.; Timimi, B. A.; Luckhurst, G. R.; Bruce, D. W. *J. Am. Chem. Soc.* **2001**, *123*, 10115.
(39) Shimizu, Y.; Kurobe, A.; Monobe, H.; Terasawa, N.; Kiyohara, K.; Uchida, K. *Chem. Commun.* **2003**, 1676.
(40) Date, R. W.; Bruce, D. W. *J. Am. Chem. Soc.* **2003**, *125*, 9012.

(41) Kouwer, P. H. J.; Mehl, G. H. *J. Am. Chem. Soc.* **2003**, *125*, 11172.
(42) Rahman, M. L.; Tschierske, C.; Yusoff, M.; Silong, S. *Tetrahedron Lett.* **2005**, *46*, 2303.
(43) Mansdorf, B. Ph.D. Dissertation, University of Akron, 2003.
(44) Wittmann, J.-C.; Lotz, B. *Makromol. Chim. Rapid Commun.* **1982**, *3*, 733.
(45) Wittmann, J.-C.; Lotz, B. *J. Polym. Sci. Polym. Phys. Ed.* **1985**, *23*, 205.
(46) Chen, J.; Cheng, S. Z. D.; Wu, S. S.; Lotz, B.; Wittmann, J.-C. *J. Polym. Sci., Polym. Phys. Ed.* **1995**, *33*, 1851.
(47) Ge, J. J.; Xue, G.; Li, C. Y.; Man, I. K.; Zhou, W. W.; Wang, S.-Y.; Harris, F. W.; Cheng, S. Z. D.; Hong, S.-C.; Zhuang, X.-W.; Shen, Y. R. *J. Am. Chem. Soc.* **2001**, *123*, 5768.
(48) Ungar, G.; Feijoo, J. L.; Percec, V.; Yourd, R. *Macromolecules* **1991**, *24*, 953.
(49) Yandrasits, A.; Cheng, S. Z. D.; Zhang, A.; Cheng, J.; Wunderlich, B.; Percec, V. *Macromolecules* **1992**, *25*, 2112.
(50) Pardey, R.; Zhang, A.; Gabori, P. A.; Harris, F. W.; Cheng, S. Z. D.; Adduci, J.; Facinelli, J. V.; Lenz, R. W. *Macromolecules* **1992**, *25*, 5060.
(51) Pardey, R.; Shen, D.; Gabori, P. A.; Harris, F. W.; Cheng, S. Z. D.; Adduci, J.; Facinelli, J. V.; Lenz, R. W. *Macromolecules* **1993**, *26*, 3687.
(52) Pardey, R.; Wu, S. S.; Chen, J.-H.; Harris, F. W.; Cheng, S. Z. D.; Keller, A.; Adduci, J.; Facinelli, J. V.; Lenz, R. W. *Macromolecules* **1994**, *27*, 5794.
(53) Yoon, Y.; Zhang, A.; Ho, R.-M.; Cheng, S. Z. D.; Percec, V.; Chu, P. *Macromolecules* **1996**, *29*, 294.
(54) Yoon, Y.; Ho, R.-M.; Moon, B.; Kim, D.; McCreight, K. W.; Li, F.; Harris, F. W.; Cheng, S. Z. D.; Percec, V.; Chu, P. *Macromolecules* **1996**, *29*, 3421.
(55) Zheng, R.-Q.; Chen, E.-Q.; Cheng, S. Z. D.; Xie, F.; Yan, D.; He, T.; Percec, V.; Chu, P.; Ungar, G. *Macromolecules* **1999**, *32*, 3574.
(56) Zheng, R.-Q.; Chen, E.-Q.; Cheng, S. Z. D.; Xie, F.; Yan, D.; He, T.; Percec, V.; Chu, P.; Ungar, G. *Macromolecules* **1999**, *32*, 6981.
(57) Iannacchione, G. S.; Mang, J. T.; Kumar, S.; Finotello, D. *Phys. Rev. Lett.* **1994**, *73*, 2708.
(58) Cammidge, A. N.; Bushby, R. J. *Handbook of Liquid Crystals*; Demus, D., Goodby, J., Gray, G. W., Spiess, H.-W., Vill, V., Eds.; Wiley-VCH: Weinheim, 1998; Vol. 2B, pp 693−748.
(59) Jeong, K.-U.; Jing, A. J.; Monsdorf, B.; Graham, M. J.; Tu, Y.; Harris, F. W.; Cheng, S. Z. D. *Chin. J. Polym. Sci.* **2007**, *25*, 57−71.
(60) Dierking, I. *Textures of Liquid Crystals*; Wiley-VCH: Weinheim, 2003.
(61) Keller, A.; Cheng, S. Z. D. *Polymer* **1998**, *39*, 4461.
(62) Cheng, S. Z. D.; Keller, A. *Annu. Rev. Mater. Sci.* **1998**, *28*, 533.
(63) Als-Nielsen, J.; Birgeneau, R. J.; Kaplan, M.; Litster, J. D.; Safinya, C. R. *Phys. Rev. Lett.* **1977**, *39*, 352.
(64) Seddon, J. M. *Handbook of Liquid Crystals*; Demus, D., Goodby, J., Gray, G. W., Spiess, H.-W., Vill, V., Eds.; Wiley-VCH: Weinheim, 1998; Vol. 1, pp 636−679.
(65) Kim, G.-H.; Pugh, C.; Cheng, S. Z. D. *Macromolecules* **2000**, *33*, 8983.
(66) Acharya, B. R.; Primak, A.; Kumar, S. *Phys. Rev. Lett.* **2004**, *92*, 145506/1.
(67) Prasad, V.; Kang, S.-W.; Suresh, K. A.; Joshi, L.; Wang, Q.; Kumar, S. *J. Am. Chem. Soc.* **2005**, *127*, 17224.
(68) Taylor, T. R.; Fergason, J. L.; Arora, S. L. *Phys. Rev. Lett.* **1970**, *24*, 359.
(69) Freiser, M. J. *Phys. Rev. Lett.* **1970**, *24*, 1041.
(70) Eashoo, M.; Wu, Z.; Zhang, A.; Shen, D.; Tse, C.; Harris, F. W.; Cheng, S. Z. D.; Gardner, K. H.; Hsiao, B. S. *Macromol. Chem. Phys.* **1994**, *195*, 2207.